Journal of Wind Engineering and Industrial Aerodynamics, 41-44 (1992) 2575–2586
Elsevier

Velocity-pressure field of cross ventilation with open windows analyzed by wind tunnel and numerical simulation

Shinsuke KATO[a], Shuzo MURAKAMI[a], Akashi MOCHIDA[a],
Shin-ichi AKABAYASHI[b] and Yoshihide TOMINAGA[a]

[a] Institute of Industrial Science, University of Tokyo,
7-22-1 Roppongi, Minato-ku, Tokyo, 106 JAPAN
[b] Faculty of Engineering, Niigata University
8050 Ikarashi 2, Niigata, 950-21 JAPAN

Abstract

In order to investigate the mechanism of cross ventilation with open windows, velocity and pressure fields of airflows in and around building models are analyzed in detail by means of wind tunnel tests and numerical simulations. Large eddy simulation (LES) is used for 3D turbulent flow analysis. The results of LES agree very well with those of the wind tunnel tests, and thus the accuracy of the numerical method used here is well validated. By means of LES, the spatial distributions of mean static pressure, turbulence energy, turbulence energy dissipation rate, etc. are examined with sufficient accuracy.

The energy dissipating process (total pressure loss) along a cross flow through a building model is examined in relation to the conventional method for predicting the airflow rate of wind-induced ventilation, which uses static pressure drops and the discharge coefficients α of openings. However, in cross ventilation with large openings, the dynamic pressure which has a significantly large value in a room, cannot be neglected. Therefore we cannot predict the airflow rates with the conventional method based on static pressure drops. The airflow through large openings still preserves much of its mean kinetic energy when it remains inside the room and this is reflected in decreased values of the total pressure loss coefficients.

NOMENCLATURE

x_i : three components of spatial coordinate
(i=1, 2, 3 : streamwise, lateral, vertical)
$\langle f \rangle$: time-averaged value of f
$\bar{f}$: filtered value of f
f' : deviation from $\langle f \rangle$
H_b : height of building model
P : pressure (static pressure)
P_o : reference static pressure
P_t : total pressure
$\frac{1}{2}\rho\langle u \rangle^2$, $\frac{1}{2}\rho(\frac{Q}{A})^2$: dynamic pressure in stream tube
u_i : three components of velocity vector
u_b : u_i value at H_b
ν_{SGS} : SGS(subgrid-scale) eddy viscosity
ε : turbulence energy dissipation rate
$(\doteqdot \langle \nu_{SGS} \frac{\partial u_i}{\partial x_j}\left(\frac{\partial u_i}{\partial x_j}+\frac{\partial u_j}{\partial x_i}\right)\rangle)$
K: mean kinetic energy
k : turbulent kinetic energy $(\frac{1}{2}\langle u'_i u'_i \rangle + k^*)$
k^* : SGS turbulent kinetic energy
$(=\nu_{SGS}/(C_k h)^2,\ C_k = 0.086)$
τ_W : wall shear stress
h : mesh interval
h_n : mesh interval adjacent to solid wall
$(u_i)_n$: tangential component of velocity vector at near-wall node
A : area of opening
Q : airflow rate
C_p : wind pressure coefficient $(=(P-P_o)-\frac{1}{2}\rho\langle u_b \rangle^2)$
ζ : total pressure loss coefficient
α : discharge coefficient $(=1/\sqrt{\zeta})$
LP : lost power in control volume

Values are made dimensionless by $\langle u_b \rangle$, H_b and ρ.

1. INTRODUCTION

The airflows in and around a building with open windows are very complicated. In order to investigate the mechanism of cross ventilation with open windows, these complicated velocity and pressure fields both in and around the building must be analyzed in detail. Although wind tunnel testing is a very reliable tool for analyzing these airflows, it has certain limitations; for example, it is difficult to analyze the spatial distributions of mean static pressure, 3D mean velocity, turbulence energy, and turbulence energy dissipation rate by means of this method.

Several researchers including the present authors have clarified that large eddy simulation (LES) is one of the most promising methods for analyzing such complicated 3D turbulent flows with sufficient accuracy [1, 2, 3]. Hence LES is used for investigating the velocity and pressure fields of cross ventilation with open windows in this study.

The energy dissipating process along a cross flow is examined in detail by means of numerical simulation in relation to the conventional and simple method of calculating airflow rate of wind-induced ventilation, which is usually based on the total pressure loss expressed by Bernoulli's law along a stream tube. In this conventional method, followings are assumed: (1) a discharge coefficient α of a opening is assumed to be a known value given by the experiments using a comparatively small opening and usually given as a constant. (2) The driving force for cross ventilation is given as the total pressure difference between the inflow and outflow openings of a building model, and it is assumed that this can substituted for the static pressure difference in the belief that dynamic pressure can be neglected. (3) The total pressure difference between the wind- and lee-ward surfaces of a building model with no openings is assumed to be hardly affected by the arrangement of the openings.

In this study particular attention is paid to the inadequacy of the above mentioned assumptions. All of them are clearly related to the energy dissipation process of cross ventilated airflow. For the precise calculation of the total pressure loss coefficient by LES, a new model called "Energy Balance Model" which evaluates the airflow rates in flow networks [6, 7] is introduced [8].

2. BUILDING MODELS AND CASES ANALYZED

Fig. 1 shows a schematic view of the basic building model (Model 2). Each opening is in contact with the floor. The ratio of the opening area to each wall plane is confined to about 6 % and the openings thus have little influence on the airflows around the building model [4]. Table 1 shows the types of models analyzed here. Model 1 has a duct connecting the inflow and outflow opening. Models 2 and 4 have thick walls and Models 3 and 5 have thin walls. Models 4 and 5 have windbreak panels so as to diffuse the inflow jet. The discharge coefficient of an opening is conventionally measured under the assumption that the total pressure loss through the opening is identical with the static pressure loss because the air on either side of the opening is stagnant with a small distance away from the opening and thereby the jet through the opening dissipates all its mean kinetic energy by turbulent mixing with ambient air. In the models used here (modeled by considering the scale ratio of real

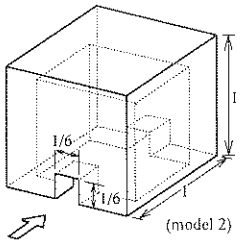

Fig. 1. Schematic view of model

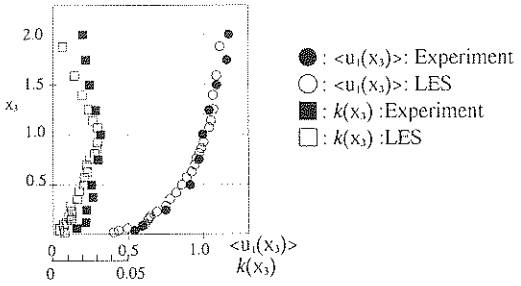

Fig. 2. Vertical profile of approaching wind

Table 1. Types of models analysed

Model 1	Model 2	Model 3	Model 4	Model 5
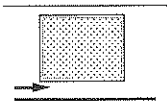	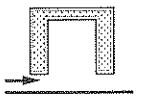	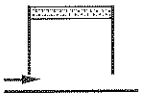	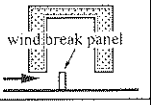	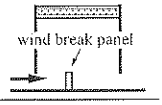
Tunnel type : windward and leeward wall is connected by a square duct of 1/6 × 1/6	Thick orifice type : Thickness of the wall is 1/6	Thin orifice type : thickness of the wall is 1/60	Thick orifice type with wind break : similar to model 2 but with a wind break panel	Thin orifice type with wind break : similar to model 3 but with a wind break panel

housing), the distance between the inflow and outflow openings is too short for the inflow jet to dissipate its mean kinetic energy before it reaches the outflow opening, but a windbreak is installed so that the inflow air dissipates its mean kinetic energy thoroughly in the room.

In this study, when physical quantities such as velocity, length, pressure etc. are expressed non-dimensional form, they are divided by the representative values. The representative values used are the height of the model building, H_b, the air velocity at the height of building model, $\langle u_b \rangle$, and the density of air, ρ .

3. OUTLINE OF WIND TUNNEL TESTS

The vertical mean velocity profile of approaching wind follows the power law, $\langle u_1 \rangle \propto x_3^{1/4}$ as shown in Fig. 2. The height of the building model used is 18cm.

Airflow rate was measured by the tracer gas method[8]. An electric manometer (capacitance manometer) was used to measure the static pressure at the floor and the wall. Wind velocity was measured by a thermistor anemometer and a tandem-type hot-wire anemometer which can discern 3D components of velocity vector[8].

4. OUTLINE OF NUMERICAL SIMULATION

Turbulent flow simulation was conducted based on Large Eddy Simulation (LES). The governing equations for LES are shown in Table 2. A Smagorinsky subgrid model is applied in LES, where the Smagorinsky coefficient is given as a variable following eq.(4) [9, 10]. Numerical simulation with the variable Smagorinsky coefficient seems to have higher potential to describe many sorts of turbulent flows

Table 2. Model equations for LES [9]

$$\frac{\partial \overline{u_i}}{\partial x_i}=0 \quad \cdots\cdots(1) \qquad \frac{\partial \overline{u_i}}{\partial t}+\frac{\partial \overline{u_i}\overline{u_j}}{\partial x_j}=-\frac{\partial P/\rho}{\partial x_j}+\frac{\partial}{\partial x_j}\left\{(\nu+\nu_{SGS})\left(\frac{\partial \overline{u_i}}{\partial x_j}+\frac{\partial \overline{u_j}}{\partial x_i}\right)\right\} \quad \cdots\cdots(2)$$

$$\nu_{SGS}=(C_S h)^2 S \quad \cdots\cdots(3) \qquad \frac{C_S}{C_{S0}}=1-C_A\frac{DS/Dt}{S^2} \quad \cdots\cdots(4) \qquad S=\left[\left(\frac{\partial \overline{u_i}}{\partial x_j}+\frac{\partial \overline{u_j}}{\partial x_i}\right)^2/2\right]^{1/2} \quad \cdots\cdots(5)$$

$$\frac{D}{Dt}=\frac{\partial}{\partial t}+\overline{u_j}\left(\frac{\partial}{\partial x_j}\right) \quad \cdots\cdots(6) \qquad C_{S\min}<C_S<C_{S\max}$$

$$C_{S\min}=0.0,\ C_{S\max}=0.27,\ C_{S0}=0.16,\ C_A=1.8$$

Table 3. Boundary conditions[2]

inflow	$\overline{u_1(t)}$, $\overline{u_2(t)}$, $\overline{u_3(t)}$:time history of velocity in boundary layer of plane channel predicted by LES. ($\langle\overline{u_1(x_3)}\rangle \fallingdotseq x_3^{1/4}$, $\langle\overline{u_2(x_3)}\rangle = 0$, $\langle\overline{u_3(x_3)}\rangle = 0$)		
outflow	$\overline{u_1}$, $\overline{u_2}$, $\overline{u_3}$: free slip		
upper face of computational domain	$\overline{u_1}$, $\overline{u_2}$: free slip, $\overline{u_3}=0$	side faces of computational domain	$\overline{u_1}$, $\overline{u_3}$: free slip, $\overline{u_2}=0$
solid wall	$\tau_W=\langle\tau_W\rangle\times\frac{(\overline{u_t})_P}{\langle(\overline{u_t})_P\rangle}$ (7) $\langle\tau_W\rangle$ is estimated by equation (8). $\frac{\langle(\overline{u_t})_P\rangle}{\langle\tau_W\rangle}(C_\mu^{1/2}k_P)^{1/2}=\frac{1}{\kappa}\ln\left(\frac{E\cdot 1/2h_P(C_\mu^{1/2}k_P)^{1/2}}{\nu}\right)$ (8) $\langle(u_t)_P\rangle$, k_P are given by using the results of the foregoing time steps.		

[9, 10, 11]. Detail of the numerical method is shown in ref.[1].

The computational domain covered $15.7H_b$ (x_1-direction) by $9.7H_b$ (x_2-direction) by $5.2H_b$ (x_3-direction). This domain is divided into $61(x_1) \times 47(x_2) \times 38(x_3)$. The interior of the model building is divided into $24(x_1)$,$21(x_2)$,$23(x_3)$. The opening area is divided into $5(x_2) \times 8(x_3)$. The finest mesh interval which is set adjacent to the solid wall was $1/50H_b$. Boundary conditions are summarized in Table 3. For the inflow boundary, time history of $u_1(t)$ in a boundary layer of a fully developed channel flow predicted by LES was used. It is slightly modulated so as to satisfy the condition that its time averaged vertical profile follows the power law ($\langle u_1(x_3)\rangle \propto x_3^{1/4}$).

5. VELOCITY FIELDS

5.1. Velocity vector fields

Figs. 3 and 4 show time-averaged velocity vector fields. Figures of the results of Models 2 and 4 are omitted since the results are nearly the same with those of Models 3 and 5, respectively. The correspondence between LES and the experiment is fairly good (ex. Fig.3-(1)-(a) and Fig.4-(1)-(a), Fig.3-(2)-(a) and Fig.4-(1)-(a)). The flowfields of each model differ little from each other. A reverse flow along the ground is commonly observed just in front of the inflow opening. That is, the approaching airflow near the ground is not induced into the building model. Air above and in front of the opening becomes a downdraft and flows into the opening. At the outflow opening, the discharged jet is induced upward by the recirculating flow in the building wake.

Inflow into the room is contracted at the openings. In Models 2 and 3 large scale

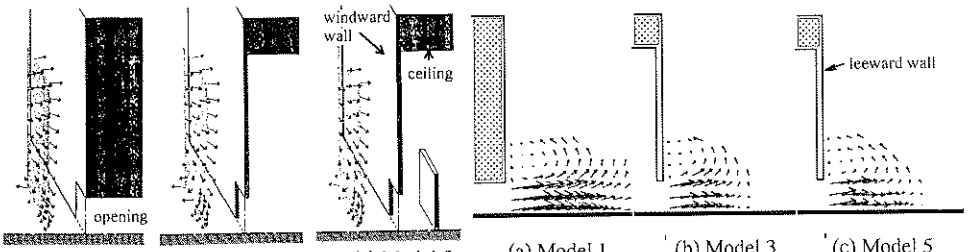

Fig. 3. Distribution of velocity vectors (Experiment). $\langle u_b \rangle$: ⟶

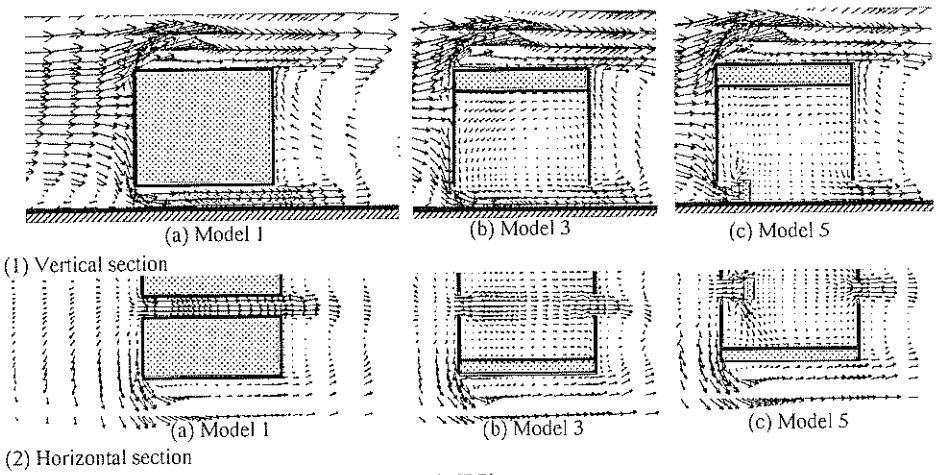

Fig. 4. Distribution of velocity vectors (LES). $\langle u_b \rangle$: ⟶

recirculating flows are observed in the rooms. In Models 4 and 5 inflows collide with windbreaks and are diffused. In Models 1, 2, and 3 inflow jets seem to flow out of the room with almost no decrease in velocity, however, in Models 4 and 5 stagnant room air accelerates in front of the outflow opening and then flows out.

5.2.Scalar velocity fields

Fig. 5 shows contour lines of the time-averaged scalar velocity given by LES. Figures of the result of Models 2 and 4 are also omitted. High velocity regions are observed at the upper front and side corners of the models. In Models 1, 2 and 3, room air has also high velocity along the virtual stream tube [8] from the inflow opening to the outflow opening. In particular, in Models 2 and 3 inflow jets hardly diffuse and flow directly out of the rooms. In these cases, the virtual stream tubes in the rooms have the fine width as the inflow opening. However, in Models 4 and 5 the inflow jets are diffused thoroughly by the windbreaks and consequently converging flows appear in front of the outflow openings. The virtual stream tubes in the rooms then become as wide as the room.

Fig. 6 show the vertical distribution of the scalar velocity and the velocity component. Here, the correspondence between LES and the experiment is good. The

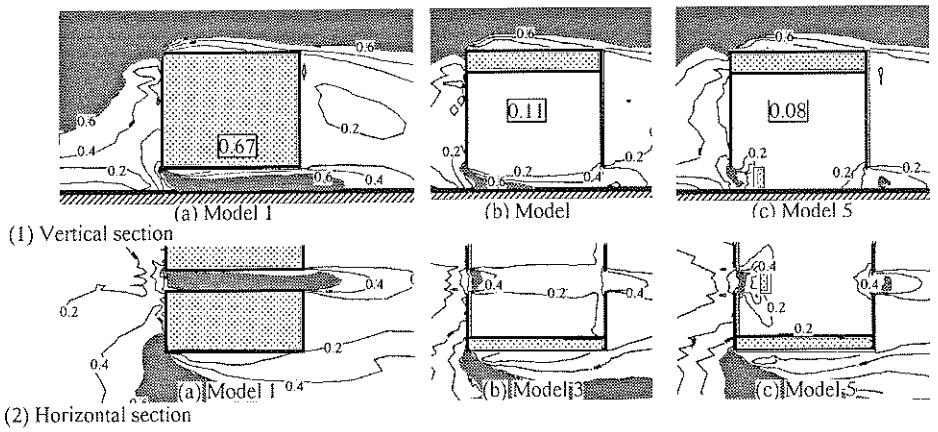

Fig. 5. Distribution of scalar velocity (LES).

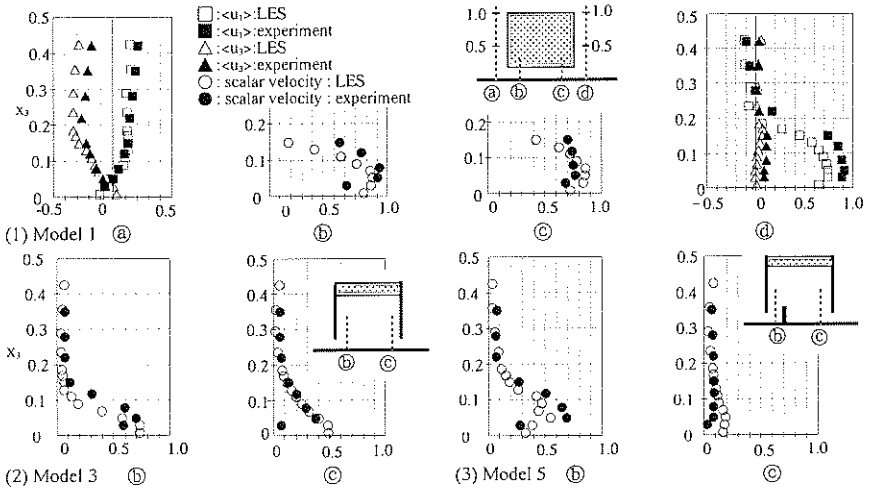

Fig. 6. Vertical distribution of velocity (Experiment and LES).

small discrepancies between them may be attributed to the coarseness of the mesh dividing near the floor.

In Models 2 and 3 two different regions can be clearly observed(Fig. 5-(1)-(b), Fig. 6-(2)); one is a high velocity region which corresponds to the inflow jet near the floor and the other is the remaining stagnant flow region. In Models 4 and 5 the boundary between the two regions becomes unclear because of the windbreak (Fig. 5-(1)-(c), -(2)-(c), Fig. 6-(3)-ⓒ).

In cross ventilation, inflow jets from the windows soon reach the opposite side wall and there is little time for their mean kinetic energy to diffuse and dissipate inside the room. Therefore, if there are no objects in the room and the inflow jets are smoothly exhausted from the outflow windows, a major part of their total energy which is estimated from the product of the total pressure and the airflow rate is

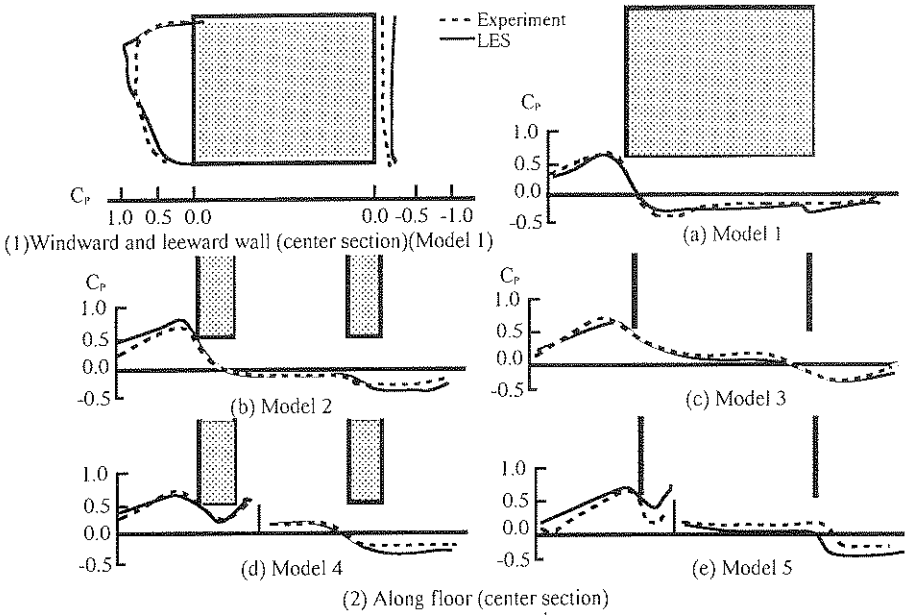

Fig. 7. Wind pressure coefficient, C_P (= $<P-P_0>/\frac{1}{2}\rho<u_b>^2$)(Experiment and LES)

preserved. According to the concept used in the conventional method, a turbulent jet discharged into stagnant space through a opening is assumed to lose its mean kinetic energy completely, but such modeling is by no means correct in cross ventilation with open windows. Models 4 and 5 have windbreaks which are installed so as to make their mean kinetic energy to be dissipated within a short distance.

5.3. Airflow rate

In table 5, the airflow rates Q of the cross ventilation are tabulated. The correspondence between LES and the experiment is very good. Model 1 has the largest airflow rate and Model 5 the smallest. The airflow rate of Model 2 was larger than that of Model 4, which has a windbreak inside the room. A difference of airflow rate is also observed between Model 5 and Model 3. This suggests that a short distance between the inflow and outflow openings — here only six times the width of the opening — is insufficient for dissipation of inflow jet kinetic energy within the room.

6. PRESSURE FIELDS

6.1.Wind pressure of wall

Fig. 7-(1) shows the distribution of the wall surface pressure coefficient of Model 1. Since the wall surface pressure coefficients of the five Models are the same, figures of the other cases are omitted. The correspondence between the experiment and the simulation is good at the windward wall. However, at the leeward wall there is a common tendency in all models for LES to show a little larger negative pressure than the wind tunnel test. The reason for this tendency, which appears in other studies

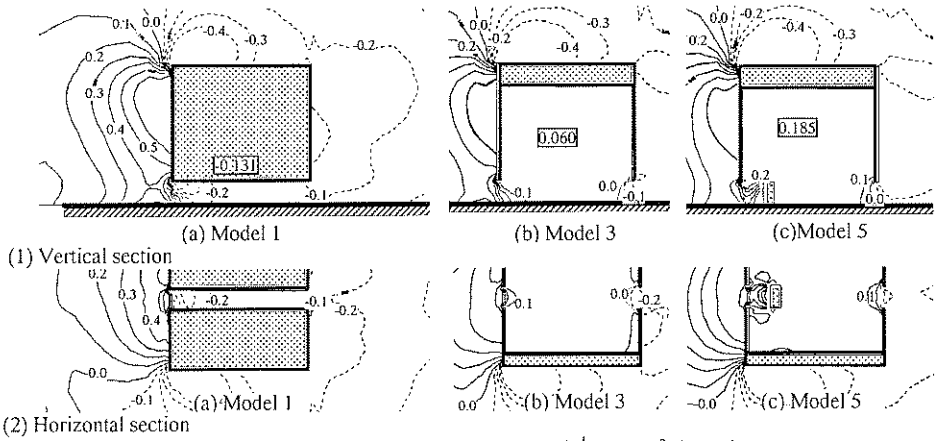

Fig. 8 Spatial distribution of static pressure $\langle P-P_0\rangle / \frac{1}{2}\rho\langle u_0\rangle^2$ (LES).

by the present authors, has not yet been clarified. It should be noted that the approaching wind in LES is not exactly the same as that in the wind tunnel test, as shown in Fig. 2.

6.2.Floor static pressure distribution

Fig. 7-(2) shows the distribution of floor surface pressure (normalized by the dynamic pressure at the model height). The correspondence between LES and the experiment is in general very good.

As shown in Fig. 7-(2), although the static pressure levels both in front of and behind the models are the same in all models, the static pressure within the rooms differs greatly. In Model 1, the static pressure in the room is almost the same as that in the wake region. The static pressure in the room becomes larger in the cases where the airflow rates are smaller (namely, models 4 and 5, cf. Table 5 & Fig. 7), that is, the static pressure drop at the outflow opening is largest when the airflow rate is smallest. The discharge coefficient α of the outflow opening (the total pressure loss coefficient ζ) is the same in all models because of the identical shape of the opening. The airflow rate is calculated as the product of the discharge coefficient and the opening area and the square root of the total pressure loss which is usually substituted for by the static pressure loss. That is, the larger static pressure drop means the larger airflow rate. In this context, this reverse phenomenon, that is, the larger static pressure the smaller airflow rate suggests that the static pressure drop does not represent the total pressure drop (because the total pressure drop is directly related to the airflow rate) and therefore the static pressure does not represent the total pressure of the room. The conventional airflow rate calculation based on the discharge coefficient and the static pressure difference thus cannot be used in this case.

When the airflow passes the outflow opening, if it preserves a certain amount of mean kinetic energy, the need to the transform static into dynamic pressure is not so large. If it has lost all mean kinetic energy, the need to transform static into dynamic pressure is very large. In Models 4 and 5, the inflow jets have lost their kinetic energy entirely; therefore they must have had higher static pressure inside the room to be lost by transformation into dynamic energy when passing through the outflow opening. This higher static pressure inside the room means a smaller static pressure difference

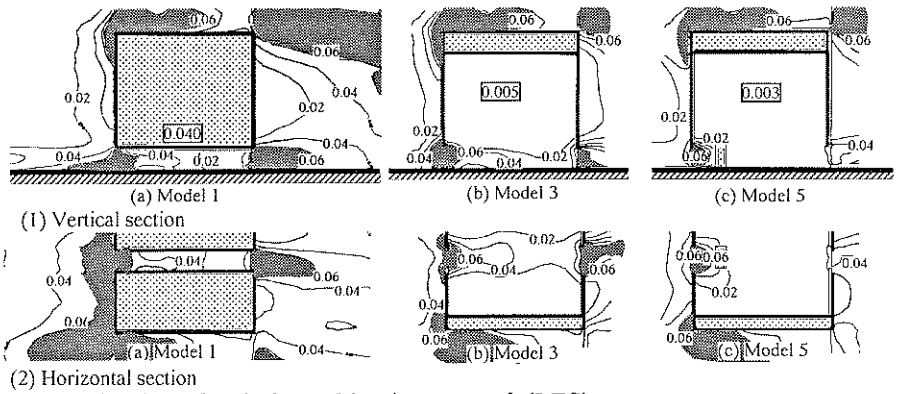

Fig. 9. Distribution of turbulence kinetic energy k (LES).

at the inflow opening and consequently a lower airflow rate.

6.3. Spatial distribution of mean static pressure

Fig. 8 shows the spatial distribution of time-averaged static pressure obtained from LES. The outer distribution pattern of the static pressure of each Model is almost identical. A high pressure region appears in front of the windward wall and a negative low pressure region appears at the flow separation point at the frontal edge of the models. The negative pressure gradually recovers during the flow downwards.

At the inflow opening a region of strong negative pressure gradient appears with the acceleration of the airflow into the room. This negative pressure gradient becomes small in Models 4 and 5, since the airflow rate is small in these models. On the other hand, a quite strong negative pressure gradient appears at the outflow openings in Models 4 and 5.

7. ENERGY FIELD OBTAINED FROM LES

7.1. Kinetic energy k

Fig. 9 shows the distribution of turbulence kinetic energy k obtained from LES. Illustration of the distribution of mean kinetic energy is omitted since its characteristics can be easily analyzed from the distribution of the time-averaged scalar velocity (Fig. 5). Turbulence kinetic energy is produced by the mean velocity gradient and shear stress. High values of turbulence kinetic energy are observed in the region where the mean velocity gradient is steep: at the frontal corner of the building model, at the inflow opening, and in the discharged flow from outflow opening.

7.2. Turbulence energy dissipation rate ε

Fig. 10 shows the distribution of turbulence energy dissipation rate ε obtained from LES. The turbulence energy dissipation rate resembles the turbulence energy in its distribution. It has high values in the regions where the turbulence energy also has high values. Since turbulence energy dissipation is directly related to the total pressure loss, total pressure loss of the cross ventilation mainly occurs in these areas.

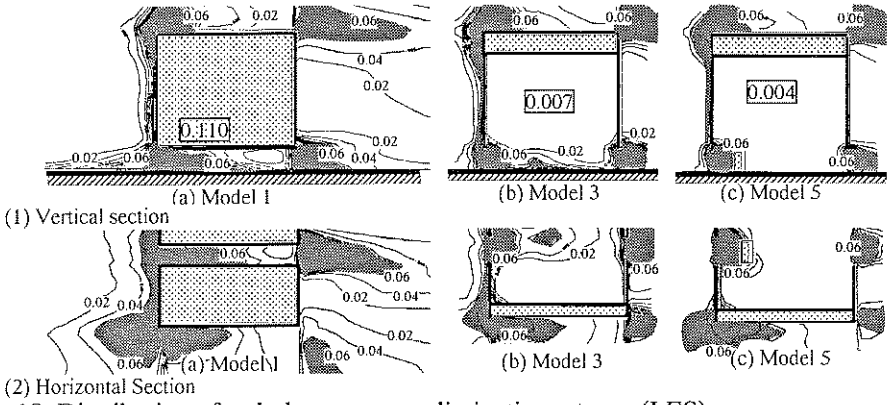

Fig. 10. Distribution of turbulence energy dissipation rate ε (LES).

7.3 Energy loss and total, static pressure drop

7.3.1. Energy balance equation

Total pressure and its loss can be defined along a virtual stream tube. However, the flowfield of cross ventilation is too complicated to define the virtual stream tube easily. In order to precisely analyze the structure of the total pressure loss, the energy balance of the flowfield is examined. The total pressure loss corresponds to the energy loss of the flowfield and the energy field is predicted accurately by LES.

Eq. (9) in Table 4 is the fundamental equation for calculating airflow rate in a flow network [6, 7, 8] and expresses the energy balance of the flowfield. It is an integrated version of the exact kinetic energy conservation equation derived from the original N-S equations. The energy loss (term LP, ③ in eq.(9)), the summation of mean kinetic energy transport (① in eq. (9)) and the summation of pressure work (② in eq. (9)) are balanced in total. As shown in eq. (12) the term LP consists of the volume integration of turbulence energy dissipation rate and other terms. Usually, LP approximately corresponds to the integration of the turbulence energy dissipation rate (① ,eq.(12)), since the remaining terms (② ~ ⑥ , eq.(12)) can be neglected[8]. If the flow geometry has only one inflow opening and one outflow opening, a virtual stream tube connecting the two opening can be assumed and this term LP corresponds to the product of total pressure loss and airflow rate (cf. the note of Table 4). In this case, the sum of pressure work also equals the product of the static pressure drop and the airflow rate.

7.3.2. Static and total pressure loss

In table 5, the airflow rate Q(Ⅰ , Ⅱ in Table. 4), the sum of pressure work $\int U_n(p/\rho)ds$(Ⅲ) and the volume integration of turbulence energy dissipation rate $\int \varepsilon dv$(Ⅴ) are tabulated. Two types of airflow rates are compared. One is given from the experiment (Ⅱ) and the other from LES (Ⅰ). The sum of pressure work and the integration of turbulence energy dissipation rate are obtained only from LES. Except for Model 1, the sum of pressure work (Ⅲ) is almost balanced with the integration of the energy dissipation rate (Ⅴ) since the first term, ① of eq. (9) in Table 4 is zero because inflow and outflow openings have the same area. Except for Model 1, the

Table 4 Energy balance model for flow networks[6]

$$\sum_m Q_m \frac{1}{2}\left(\frac{Q_m}{A_m}\right)^2 + \sum_m Q_m (P/\rho)_m + LP = 0 \quad (9), \quad LP = \sum_m \xi_m Q_m \frac{1}{2}\left(\frac{Q_m}{A_m}\right)^2 \quad (10), \quad \sum_m Q_m = 0 \quad (11)$$

① ② ③

Here, LP (lost power) is expressed as follows

$$LP = \{\nu\overline{\left(\frac{\partial U_i}{\partial X_i}\right)^2} + \varepsilon\} \cdot V - \sum_m \overline{\frac{\partial (K+k)}{\partial X_n}}_m A_m + \sum_m \overline{(u_n u_i u_i + u_n p/\rho)}_m A_{in} + \sum_m \overline{U_{im}(u_i u_n)}_m A_m$$

① ② ③ ④

$$- \sum_m \{\overline{U_{nm}}(K+k)_m A_m - Q_m \frac{1}{2}\left(\frac{Q_m}{A_m}\right)^2\} + \sum_m \{\overline{U_{nm}(P/\rho)}_m A_m - Q_m (P/\rho)_m\} \quad (12)$$

⑤ ⑥

• Eq.(9) ,(10), and (11) are the fundamental equations of Energy Balance Model for analyzing flow networks. Eq.(9) expresses the energy balance in the control volume and eq.(11) expresses the continuity balance. Eq.(9) is an integrated version of the exact energy preservation equation derived from the N-S equation [8]. Q_m has a positive value when air flows out of the control volume.

• over-bar in eq.(12) means volume or area average.

• m is index for each opening of the control volume. It is possible for m to exceed 2. If the number of openings is two, it is easy to assume a virtual stream tube where the flow rate is the same but has the opposite sign ($Q_1 = -Q_2$) and eq.(9) reduces to the familiar form of the Bernoulli's law multiplied by flow rate Q .

• ①, ②, ③ in eq.(9) are proportionate to dynamic pressure, static pressure and total pressure loss, respectively).

• Physical dimension of the variables are follows;

ρ :[kg/m^3], Q : [m^3/s], A : [m^2], k, K : [m^2/s^2], ε : [m^2/s^3], ν : [m^2/s]

P(static pressure) : [N/m^2], $\frac{1}{2}\rho\left(\frac{Q}{A}\right)^2$(dynamic pressure) : [kg/ms^2 = N/m^2]

$Q\frac{1}{2}\rho\left(\frac{Q}{A}\right)^2$(kinetic energy convection) : [N·m/s = W], $Q\frac{1}{2}\left(\frac{Q}{A}\right)^2$: [m^3·W/kg = m^3·m^2/s^3],

$\frac{1}{2}\left(\frac{Q}{A}\right)^2$: [m^2/s^2 = Nm/kg]

QP (pressure work) : [N·m/s = W], $Q(P/\rho)$: [m^3· W/kg = m^3· m^2/s^3],

$\int U_n(P/\rho)ds/Q \approx P/\rho$ = [m^2/s^2 = N·m/kg]

$\rho \cdot LP \approx \rho \cdot \int \varepsilon dv$ (energy dissipation) :[kg·m^2/s^3 = N·m/s = W], $LP \approx \int \varepsilon dv$ =[m^3·W/kg=m^3·m^2/s^3]

If a virtual stream tube can be assumed, $\Delta P_t/\rho = LP/Q \approx \int \varepsilon dv/Q_t$ = [m^2/s^2 = N·m/ kg]

Table 5. Flow rate, pressure work, turbulence energy dissipation rate

	I	II	III *	IV **	V	VI ***
	Q_t (LES)	Q_n (experiment)	$\int U_n(p/\rho)ds$ ($\approx \sum_m Q_m(P/\rho)_m$) (LES)	$\int U_n(p/\rho)ds/Q_t$ ($\approx \Delta P/\rho$) (LES)	$\int \varepsilon dv$ ($\approx$LP) (LES)	$\int \varepsilon dv/Q_t$ ($\approx \Delta P_t/\rho$) (LES)
Model 1	0.021	0.023	0.001	0.05	0.003	0.14
Model 2	0.019	0.019	0.003	0.16	0.005	0.26
Model 3	0.016	0.014	0.004	0.25	0.005	0.31
Model 4	0.017	0.015	0.006	0.35	0.005	0.29
Model 5	0.011	0.012	0.002	0.18	0.003	0.27

* : Integration is conducted for the area enclosed by outer boundary surface of model. The terms ⑤ and ⑥ in eq.(12) of Table 4 can be assumed to be zero.

** : In this case, $\int U_n(p/\rho)ds/Q$ corresponds to the static pressure drop $\Delta P/\rho$ between the outer windward opening surface and the outer leeward opening surface.

***: In this case, $\int \varepsilon dv/Q$ corresponds to the total pressure drop $\Delta P_t/\rho$ between the two openings.

estimated total pressure loss in the room ($\int \varepsilon dv/Q \approx \Delta P_t/\rho$, VI) is almost the same. The estimated static pressure drop($\Delta P/\rho$, IV) of each model is different. Except for Model 5 these estimated static pressure drops ($\Delta P/\rho$, IV) corresponds well to the static pressure differences between the room and the wake region (cf. Fig. 8). Since the static pressure changes greatly along the flow and energy loss occurs abruptly around the opening, and because mesh dividing for LES around here is not fine enough, the

estimated static and total pressure might have some errors. However, it is obvious that in neither types does the static pressure drop ($\Delta P/\rho$, IV) correspond to the total pressure drop ($\Delta P_t/\rho$, VI) and it is thus clear that in this type of flowfield the total pressure drop $\Delta P_t/\rho$ cannot be substituted for the static pressure drop $\Delta P/\rho$.

8. CONCLUSIONS

1. The results of LES agree well with those of the wind tunnel test and thus the numerical method is well validated.
2. LES enables us to analyze the velocity and pressure fields of complicated 3D flow in detail. In particular, it make it possible to analyze the space distributions of mean static pressure, turbulence energy, and turbulence energy dissipation rate with sufficient accuracy.
3. The energy dissipating process along a cross flow through a building model is examined from the static and total pressure drop. The static pressure in the room by no means represents the total pressure and therefore the conventional airflow rate calculation method based on the discharge coefficient of openings and static pressure differences can hardly be applied to such types of flowfields, since the inflow jets from the inflow openings preserve some of their kinetic energy until they are exhausted from the outflow openings.

REFERENCES

1 S. Murakami, Numerical simulation of turbulent flowfield around cubic model current status and applications of k- ε model and LES, J. Wind Eng. Ind. Aerodyn., 33 (1990) 139-152.
2 S. Murakami and A. Mochida and Y. Hayashi, Examining the k- ε model by means of a wind tunnel test and large eddy simulation of the turbulence structure around a cube, J. Wind Eng. Ind. Aerodyn., 35 (1990) 87-100.
3 S. Murakami, and A. Mochida and Y. Hayashi, S. Sakamoto, Prediction of velocity-pressure field and wind forces around bluff bodies by k- ε , ASM and LES, (submitted for 8th International Conference on Wind Engineering), (1991).
4 B.J. Vickery and C. Karakatsanis, External pressure distributions and induced internal ventilation flow in low-rise industrial and domestic structures, ASHRAE Transactions, Vol.93, Part 2 (1987) 2198-2213.
5 M.V. Swami and S. Chandra, Correlations for pressure distribution on buildings and calculation of natural-ventilation airflow, ASHRAE Transactions, Vol.94, Part 1 (1988) 243-266.
6 S.E. Guffey and D.A. Fraser, A power balance model for converging and diverging flow junctions, ASHRAE Transactions, Vol. 95 Part 2 (1989) 2-9.
7 S.E. Guffey and D.A. Fraser, Kinetic power model of junction losses, ASHRAE Transactions, Vol. 95 Part 2 (1989) 10-22.
8 S. Murakami, S. Kato, S. Akabayashi, K. Mizutani, and Y.D. Kim, Wind tunnel test on velocity -pressure field of cross ventilation with open windows,ASHRAE Transactions,Vol.97, Part1 (1991).
9 A. Yoshizawa, Eddy-viscosity-type subgrid-scale model with a variable smagorinsky coefficient and its relationship with the one-equation model in large eddy simulation, Phys. Fluid (1991).
10 A. Yoshizawa, Subgrid-scale modeling with a variable length scale, Phys. Fluid, A1 (1989) 1293-1295.
11 K. Mizutani, S.Murakami, S. Kato and A. Mochida, Numerical simulation of room air flow by means of large eddy simulation (part 1, 2), Summaries of technical papers of annual meeting, Architectural Institute of Japan, (to be submitted)(1991).